Journal of Sound and Vibration 327 (2009) 271–284

Contents lists available at ScienceDirect

Journal of Sound and Vibration

journal homepage: www.elsevier.com/locate/jsvi

Rapid Communication

# Free vibration analysis of arbitrarily shaped polygonal plates with simply supported edges using a sub-domain method

Sang Wook Kang [a,*], S.N. Atluri [b]

[a] Department of Mechanical Systems Engineering, Hansung University, 389, 2-ga, Samsun-dong, Sungbuk-gu, Seoul 136-792, Republic of Korea
[b] Department of Mechanical and Aerospace Engineering, University of California, Irvine, USA

ARTICLE INFO

*Article history:*
Received 6 March 2009
Received in revised form
15 July 2009
Accepted 17 July 2009
Handling Editor: L.G. Tham
Available online 8 August 2009

ABSTRACT

As an extension of the NDIF method developed by the authors, a practical analytical method for the free vibration analysis of a simply supported polygonal plate with arbitrary shape is proposed. Especially, the method is more effective for plates highly concave shapes because it employs a sub-domain method dividing the plate of interest with two sub-plates. The approximate solution of each sub-plate is assumed by linearly superposing plane waves propagated from edges of the sub-plate. Sub-system matrix equations for the two sub-plates are extracted by applying the simply supported boundary condition to the edges of each sub-plate (excepting the common interface of the two sub-plates). Finally, the sub-system matrix equations is merged into a single system matrix equation for the entire plate by considering the compatibility condition that the two sub-plates have the same displacement and slope at the common interface. The eigenvalues and mode shapes of the single plate are obtained from the determinant of a system matrix extracted from the entire system matrix equation. It is shown by several case studies that the proposed method has a good convergence characteristics and yields accurate eigenvalues and mode shapes, compared with another analytical method (NDIF method) and FEM (NASTRAN).



## 1. Introduction

A vast literature exists for obtaining analytical solution of free vibration of plates having no exact solution, as surveyed in the authors' previous papers [1–6], which studied analytical methods for free vibration of arbitrarily shaped plates (including arbitrarily shaped membranes and acoustic cavities). However, most investigators dealt with plates (or membranes) with special shapes such as triangle, rectangle, parallelogram, trapezoid, circle and ellipse [7–21].

On the other hand, researches [1–6,22–27] on plates with arbitrary shapes were not frequently carried out compared with plates with special shapes because most researchers consider that numerical methods such as the finite element method (FEM) [28] and the boundary element method (BEM) [29,30] are more common and easier way for objects with arbitrary shapes than analytical methods.

The authors introduced the so-called NDIF method (non-dimensional dynamic influence function method) for free vibration analysis of arbitrarily shaped membranes (or simply supported plates) [1]. Furthermore, the authors studied analytical methods for arbitrarily shaped acoustic cavities [2], arbitrarily shaped membranes with highly concave edges [3], arbitrarily shaped plates with various boundary conditions [4–6] using the NDIF method.

* Corresponding author. Tel.: +82 2 760 4228; fax: +82 2 760 4329.
*E-mail address:* swkang@hansung.ac.kr (S.W. Kang).

0022-460X/$ - see front matter © 2009 Elsevier Ltd. All rights reserved.
doi:10.1016/j.jsv.2009.07.017

Unlike FEM [28] and BEM [29,30], the NDIF method need no integration procedure in its theoretical formulation because the boundary of the domain of interest is divided with only nodes (without elements). As a result, the NDIF method needs a small amount of numerical calculations and yields rapidly converged, highly accurate result. However, the NDIF method has the week point that it may have an ill-conditioned system matrix when too many nodes are used [6]. The ill-conditioned system matrix results from a falling-off in independence between basis functions occasioned when two adjacent nodes are very near to each other.

In this paper, a new analytical method that can overcome the weak point of the NDIF method is studied for free vibration analysis of arbitrarily shaped *polygonal* plates. (Note that the newly developed method is not applicable to plates with curved edges.) The present method is based on the same concept as the NDIF method in assuming an approximate solution of a plate but it employs basis functions quite different from ones used in the NDIF method. In the present method, basis functions are given by plane waves traveling from each edge of the plate of interest, which is assumed to be located on an infinite plate, and the approximate solution is assumed as a linear combination of the plane waves. Note that, in the NDIF method, basis functions are given by circular waves traveling from each node on the edges of the plate and the approximate solution is assumed as a linear combination of the circular waves.

In addition, the use of the plane waves for basis functions already attempted in the authors' previous papers [31–33] that dealt with free vibration problems of inhomogeneous rectangular membranes [31,32] and a trapezoidal membrane [33]. It may be said that the proposed approach is to extend a theoretical way used in the previous papers [31–33] to arbitrarily shaped plates, with having the same concept as the NDIF method in assuming an approximate solution [1–6].

On the other hand, the proposed method employs a sub-domain method of sub-dividing the entire domain into two sub-domains to effectively solve the free vibration problem of highly concave polygonal plates as well as convex polygonal plates. System matrix equations for the two sub-domains are obtained by considering the simply supported boundary condition at edges and they are merged as a single system matrix equation by considering the condition of the continuity in displacement and slope along the common interface of the two sub-domains. Finally, the natural frequencies and mode shapes are extracted from a system matrix included in the single system matrix equation. The validity and accuracy of eigenvalues and mode shapes found by the present method were verified by several case studies, of which the results are compared with ones given from the NDIF method or FEM (NASTRAN).

## 2. Theoretical formulation

### 2.1. Analogy of a simply supported plate to a fixed membrane

The equation of motion for the free flexural vibration of a thin plate is written as

$$D\nabla^4 w + \rho_s \frac{\partial^2 w}{\partial t^2} = 0, \tag{1}$$

where $w = w(\mathbf{r},t)$ is the transverse deflection at position vector $\mathbf{r}$, $\rho_s$ is the surface density and $D$ is the flexural rigidity expressed as $D = Eh^3/12(1-\nu^2)$ in terms of Young's modulus $E$, Poisson's ratio $\nu$ and the plate thickness $h$. Assuming a harmonic motion $w(\mathbf{r},t) = W(\mathbf{r})\,e^{j\omega t}$ in which $\omega = 2\pi f$ denotes the circular frequency, Eq. (1) leads to

$$\nabla^4 W - \Lambda^4 W = 0, \tag{2}$$

$$\Lambda = (\rho_s \omega^2/D)^{1/4} \tag{3}$$

in which $\Lambda$ is called a frequency parameter, which is a function of frequency $f$ (Hz).

Since there exists an analogy between the vibration of a polygonal plate with the simply supported boundary condition and a similarly shaped membrane with fixed edges [8,21], Eq. (2) can be reduced to the membrane equation:

$$\nabla^2 W + \Lambda^2 W = 0. \tag{4}$$

If the $i$th eigenvalue $\Lambda_i$ is obtained by solving Eq. (4), the $i$th natural frequency $f_i$ of the polygonal plate of interest may be calculated by [8,21]

$$f_i = \frac{\Lambda_i^2}{2\pi}\sqrt{\frac{D}{\rho_s}}. \tag{5}$$

### 2.2. Extraction of system matrix equations for sub-domains

In the study, an analytical method of calculating natural frequencies and mode shapes of concave polygonal plates as well as convex polygonal plates is proposed by employing a sub-domain method of dividing an entire domain into two convex domains. As shown in Fig. 1, it is assumed that a fictitious polygonal contour (solid lines) having the same shape as the concave polygonal plate of interest is located in an infinite plate. Next, the concave plate is divided into two convex

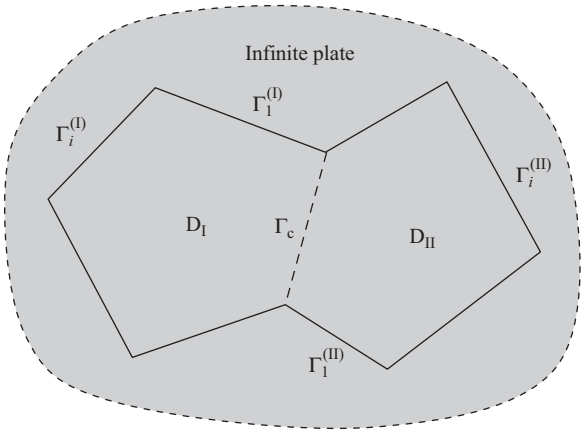


**Fig. 1.** Concave polygonal plate divided into two sub-domains $D_I$ and $D_{II}$; the plate is assumed to be located in an infinite plate.

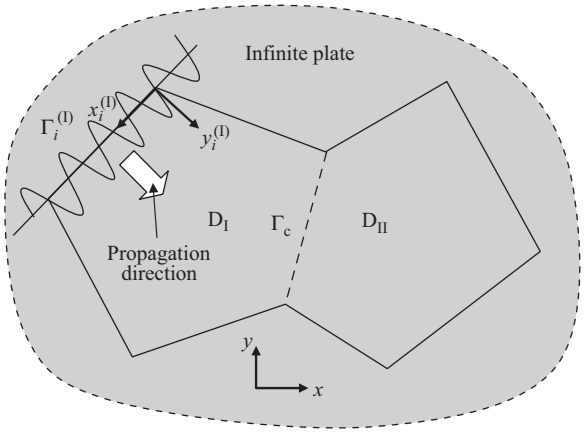


**Fig. 2.** Plane wave generated along the $i$th edge $\Gamma_i^{(I)}$ of domain $D_I$.

domains $D_I$ and $D_{II}$ which adjoin by the common interface $\Gamma_c$. It should be noted that $D_I$ is surrounded counterclockwise by edges $\Gamma_1^{(I)}, \Gamma_2^{(I)}, \ldots, \Gamma_{Na}^{(I)}$ where $\Gamma_{Na}^{(I)}$ corresponds to $\Gamma_c$ ($Na$ denotes the number of edges of the domain), and that similarly $D_{II}$ is surrounded counterclockwise by edges $\Gamma_1^{(II)}, \Gamma_2^{(II)}, \ldots, \Gamma_{Nb}^{(II)}$ where $\Gamma_{Nb}^{(II)}$ corresponds to $\Gamma_c$ ($Nb$ denotes the number of edges of the domain).

*2.2.1. System matrix equation for sub-domain* $D_I$

First, consider that a plane wave is generated along the $i$th edge $\Gamma_i^{(I)}$ of domain $D_I$ and is propagated into the inside of the plate as shown in Fig. 2. It should be noted in the figure that the direction of vibration of the plane wave is the same as the transverse deflection of the plate. Especially in the study, the plane wave is assumed as function

$$W_i^{(I)}(x_i, y_i) = \sum_{m=1}^{Ns} A_m^{(i)} \sin\frac{m\pi x_i^{(I)}}{L_i^{(I)}} \exp\left(\mathrm{j}\sqrt{\Lambda^2 - \left(\frac{m\pi}{L_i^{(I)}}\right)^2}\, y_i^{(I)}\right), \quad i = 1, 2, \ldots, Na, \tag{6}$$

where $A_m^{(i)}$ indicates unknown coefficients associated with the vibration amplitude of the plane wave; $x_i^{(I)}$ and $y_i^{(I)}$ denote local rectangular coordinates defined at edge $\Gamma_i^{(I)}$ as shown in Fig. 2; $L_i^{(I)}$, j, $Na$ and $Ns$ represent the length of edge $\Gamma_i^{(I)}$, the

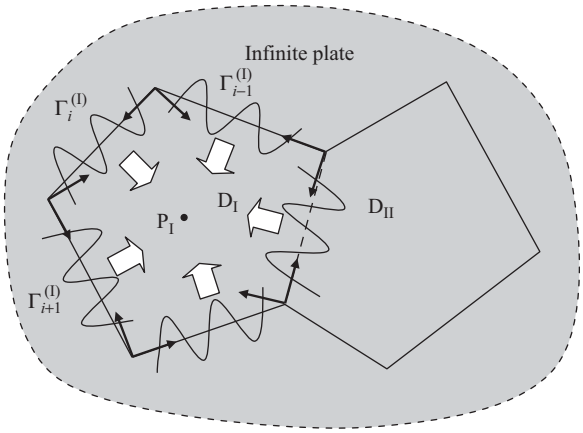


**Fig. 3.** Plane waves simultaneously generated at all edges $\Gamma_1^{(\mathrm{I})}, \Gamma_2^{(\mathrm{I})}, \ldots, \Gamma_{Na}^{(\mathrm{I})}$ of domain $D_I$.

imaginary unit ($j = \sqrt{-1}$), the number of edges (including $\Gamma_c$) of the sub-domain and the number of series functions used for the plane wave, respectively. It is important to note that Eq. (6) exactly satisfies the governing differential equation (Eq. (4)).

Next, assuming that plane waves are simultaneously generated at all edges $\Gamma_1^{(\mathrm{I})}, \Gamma_2^{(\mathrm{I})}, \ldots, \Gamma_{Na}^{(\mathrm{I})}$ as shown in Fig. 3, a displacement response at point $P_I$ in domain $D_I$ may be obtained by superposing displacements that have resulted from the plane waves. Thus, the displacement response at point $P_I$ is

$$W^{(\mathrm{I})} = \sum_{i=1}^{Na} W_i^{(\mathrm{I})}(x_i^{(\mathrm{I})}, y_i^{(\mathrm{I})}) = \sum_{i=1}^{Na}\sum_{m=1}^{Ns} A_m^{(i)} \sin\frac{m\pi x_i^{(\mathrm{I})}}{L_i^{(\mathrm{I})}} \exp\left(\mathrm{j}\sqrt{\Lambda^2 - \left(\frac{m\pi}{L_i^{(\mathrm{I})}}\right)^2}\, x_i^{(\mathrm{I})}\right). \tag{7}$$

In the paper, Eq. (7) is assumed as an approximate solution for the convex plate with the same dimensions as domain $D_I$. Note that the approximate solution exactly satisfies the governing differential equation (Eq. (4)) because $W_i^{(\mathrm{I})}(x_i^{(\mathrm{I})}, y_i^{(\mathrm{I})})$ in Eq. (7) satisfies that.

The boundary conditions for a plate with simply supported edges are given by [20]

$$W = 0 \tag{8}$$

and

$$\frac{\partial^2 W}{\partial n^2} = 0, \tag{9}$$

where $n$ represents the normal direction from the edges. Thanks to the aforementioned analogy between a simply supported plates and a fixed membrane, only the displacement-zero condition, Eq. (8), may be considered at the edges. Although displacements at all edges (with the exception of the common interface $\Gamma_c$) of the convex plate corresponding to $D_I$ are zero, displacements at all edges (including $\Gamma_c$) are provisionally assumed as a linear combination of sine series: i.e.,

$$W^{(\mathrm{I})}(x_r^{(\mathrm{I})}, y_r^{(\mathrm{I})} = 0) = \sum_{n=1}^{Ns} U_n^{(r)} \sin\frac{n\pi x_r^{(\mathrm{I})}}{L_r^{(\mathrm{I})}}, \quad r = 1, 2, \ldots, Na, \tag{10}$$

where $(x_r^{(\mathrm{I})}, y_r^{(\mathrm{I})})$ is the local rectangular coordinates defined at the $r$th edge $\Gamma_r^{(\mathrm{I})}$, $U_n^{(r)}$ denotes unknown coefficients and $L_r^{(\mathrm{I})}$ is the length of edge $\Gamma_r^{(\mathrm{I})}$.

Applying the provisional boundary condition (Eq. (10)) to the approximate solution (Eq. (7)) at edges $\Gamma_1^{(\mathrm{I})}, \Gamma_2^{(\mathrm{I})}, \ldots, \Gamma_{Na}^{(\mathrm{I})}$ (i.e., at $y_r = 0$ for $r = 1, 2, \ldots, Na$) yields

$$\sum_{i=1}^{Na} W_i^{(\mathrm{I})}(x_i^{(\mathrm{I})}, y_i^{(\mathrm{I})})|_{y_r=0} = \sum_{n=1}^{Ns} U_n^{(r)} \sin\frac{n\pi x_r^{(\mathrm{I})}}{L_r^{(\mathrm{I})}}, \quad r = 1, 2, \ldots, Na. \tag{11}$$

Next, in order to express Eq. (11) with the single local coordinate system $(x_r^{(\mathrm{I})}, y_r^{(\mathrm{I})})$ a relationship between two local coordinate systems $(x_r^{(\mathrm{I})}, y_r^{(\mathrm{I})})$ and $(x_i^{(\mathrm{I})}, y_i^{(\mathrm{I})})$ is assumed by

$$x_i^{(\mathrm{I})} = a x_r^{(\mathrm{I})} + b y_r^{(\mathrm{I})} + e \equiv f_{ir}^{(\mathrm{I})}(x_r^{(\mathrm{I})}, y_r^{(\mathrm{I})}), \tag{12}$$

$$y_i^{(\mathrm{I})} = c x_r^{(\mathrm{I})} + d y_r^{(\mathrm{I})} + h \equiv g_{ir}^{(\mathrm{I})}(x_r^{(\mathrm{I})}, y_r^{(\mathrm{I})}), \tag{13}$$

where $a$, $b$, $c$, $d$, and $h$ are constants. Substituting Eqs. (12, 13) into Eq. (11) leads to

$$\sum_{i=1}^{Na} W_i^{(\mathrm{I})}(f_{ir}^{(\mathrm{I})}(x_r, y_r=0), g_{ir}^{(\mathrm{I})}(x_r, y_r=0)) = \sum_{n=1}^{Ns} U_n^{(r)} \sin\frac{n\pi x_r^{(\mathrm{I})}}{L_r^{(\mathrm{I})}}, \quad r=1,2,\ldots,Na, \tag{14}$$

which may be concretely expressed as Eq. (15) by substituting Eq. (7) into Eq. (14):

$$\sum_{i=1}^{Na}\sum_{m=1}^{Ns} A_m^{(i)} \sin\frac{m\pi f_{ir}^{(\mathrm{I})}(x_r^{(\mathrm{I})}, y_r^{(\mathrm{I})}=0)}{L_i^{(\mathrm{I})}} \exp\left(\mathrm{j}\sqrt{\Lambda^2 - \left(\frac{m\pi}{L_i^{(\mathrm{I})}}\right)^2}\, g_{ir}^{(\mathrm{I})}(x_r^{(\mathrm{I})}, y_r^{(\mathrm{I})}=0)\right) = \sum_{n=1}^{Ns} U_n^{(r)} \sin\frac{n\pi x_r^{(\mathrm{I})}}{L_r^{(\mathrm{I})}}, \quad r=1,2,\ldots,Na. \tag{15}$$

It should be noted in the current step that Eq. (15) does not give a complete form because the geometric variable $x_r^{(\mathrm{I})}$ is included in the equation. In order to eliminate $x_r^{(\mathrm{I})}$ from Eq. (15), the $q$th basis $\sin q\pi x_r^{(\mathrm{I})}/L_r^{(\mathrm{I})}$ is multiplied to both sides of the equation and the integration procedure from 0 to $L_r^{(\mathrm{I})}$ is performed along edge $\Gamma_r^{(\mathrm{I})}$. Then, Eq. (15) leads to

$$\begin{aligned}&\sum_{i=1}^{Na}\sum_{m=1}^{Ns} \int_0^{L_r^{(\mathrm{I})}} A_m^{(i)} \sin\frac{m\pi f_{ir}^{(\mathrm{I})}(x_r^{(\mathrm{I})}, y_r^{(\mathrm{I})}=0)}{L_i^{(\mathrm{I})}} \exp\left(\mathrm{j}\sqrt{\Lambda^2 - \left(\frac{m\pi}{L_i^{(\mathrm{I})}}\right)^2}\, g_{ir}^{(\mathrm{I})}(x_r^{(\mathrm{I})}, y_r^{(\mathrm{I})}=0)\right) \sin\frac{q\pi x_r^{(\mathrm{I})}}{L_r^{(\mathrm{I})}} \mathrm{d}x_r^{(\mathrm{I})} \\ &= \sum_{n=1}^{Ns} \int_0^{L_r^{(\mathrm{I})}} U_n^{(r)} \sin\frac{n\pi x_r^{(\mathrm{I})}}{L_r^{(\mathrm{I})}} \sin\frac{q\pi x_r^{(\mathrm{I})}}{L_r^{(\mathrm{I})}} \mathrm{d}x_r^{(\mathrm{I})}, \quad q=1,2,\ldots,Ns;\ r=1,2,\ldots,Na.\end{aligned} \tag{16}$$

Due to the orthogonality of sine series, the right-hand side of Eq. (16) is simplified as

$$\sum_{n=1}^{Ns} \int_0^{L_r^{(\mathrm{I})}} U_n^{(r)} \sin\frac{n\pi x_r^{(\mathrm{I})}}{L_r^{(\mathrm{I})}} \sin\frac{q\pi x_r^{(\mathrm{I})}}{L_r^{(\mathrm{I})}} \mathrm{d}x_r^{(\mathrm{I})} = \frac{L_r^{(\mathrm{I})}}{2} U_q^{(r)} \tag{17}$$

and substituting Eq. (17) into Eq. (16) leads to

$$\begin{aligned}&\sum_{i=1}^{Na}\sum_{m=1}^{Ns} A_m^{(i)} \frac{2}{L_r^{(\mathrm{I})}} \int_0^{L_r^{(\mathrm{I})}} \sin\frac{m\pi f_{ir}^{(\mathrm{I})}(x_r^{(\mathrm{I})}, y_r^{(\mathrm{I})}=0)}{L_i^{(\mathrm{I})}} \exp\left(\mathrm{j}\sqrt{\Lambda^2 - \left(\frac{m\pi}{L_i^{(\mathrm{I})}}\right)^2}\, g_{ir}^{(\mathrm{I})}(x_r^{(\mathrm{I})}, y_r^{(\mathrm{I})}=0)\right) \sin\frac{q\pi x_r^{(\mathrm{I})}}{L_r^{(\mathrm{I})}} \mathrm{d}x_r^{(\mathrm{I})} = U_q^{(r)}, \\ &q=1,2,\ldots,Ns;\ r=1,2,\ldots,Na.\end{aligned} \tag{18}$$

For simplicity, Eq. (18) may be rewritten in a simple symbolic form:

$$\sum_{i=1}^{Na}\left(\sum_{m=1}^{Ns} A_m^{(i)} SM_{\mathrm{I}(q,m)}^{(i,r)}\right) = U_q^{(r)}, \quad q=1,2,\ldots,Ns;\ r=1,2,\ldots,Na, \tag{19}$$

where $SM_{\mathrm{I}q,m}^{(i,r)}$ is given by

$$SM_{\mathrm{I}q,m}^{(i,r)} = \frac{2}{L_r^{(\mathrm{I})}} \int_0^{L_r^{(\mathrm{I})}} \sin\frac{m\pi f_{ir}^{(\mathrm{I})}(x_r^{(\mathrm{I})}, y_r^{(\mathrm{I})}=0)}{L_i^{(\mathrm{I})}} \exp\left(\mathrm{j}\sqrt{\Lambda^2 - \left(\frac{m\pi}{L_i^{(\mathrm{I})}}\right)^2}\, g_{ir}^{(\mathrm{I})}(x_r^{(\mathrm{I})}, y_r^{(\mathrm{I})}=0)\right) \sin\frac{q\pi x_r^{(\mathrm{I})}}{L_r^{(\mathrm{I})}} \mathrm{d}x_r^{(\mathrm{I})}. \tag{20}$$

Furthermore, if separately considering the real edges of the plate ($\Gamma_1^{(\mathrm{I})}, \Gamma_2^{(\mathrm{I})}, \ldots, \Gamma_{Na-1}^{(\mathrm{I})}$) and the common interface ($\Gamma_{Na}^{(\mathrm{I})}$), Eq. (19) may be divided into two equations as follows:

$$\sum_{i=1}^{Na-1}\left(\sum_{m=1}^{Ns} A_m^{(i)} SM_{\mathrm{I}(q,m)}^{(i,r)}\right) + \sum_{m=1}^{Ns} A_m^{(Na)} SM_{\mathrm{I}(q,m)}^{(i,r)} = U_q^{(r)}, \quad q=1,2,\ldots,Ns;\ r=1,2,\ldots,Na-1, \tag{21}$$

$$\sum_{i=1}^{Na-1}\left(\sum_{m=1}^{Ns} A_m^{(i)} SM_{\mathrm{I}(q,m)}^{(i,Na)}\right) + \sum_{m=1}^{Ns} A_m^{(Na)} SM_{\mathrm{I}(q,m)}^{(Na,Na)} = U_q^{(Na)}, \quad q=1,2,\ldots,Ns. \tag{22}$$

Finally, Eqs. (21) and (22) may be simply, respectively, expressed in the form of system matrix equations as follows:

$$\mathbf{SM}_{\mathrm{I}}^{(\mathrm{bb})}\mathbf{A}_{\mathrm{I}}^{(\mathrm{b})} + \mathbf{SM}_{\mathrm{I}}^{(\mathrm{bc})}\mathbf{A}_{\mathrm{I}}^{(\mathrm{c})} = \mathbf{U}_{\mathrm{I}}^{(\mathrm{b})}, \tag{23}$$

$$\mathbf{SM}_{\mathrm{I}}^{(\mathrm{cb})}\mathbf{A}_{\mathrm{I}}^{(\mathrm{b})} + \mathbf{SM}_{\mathrm{I}}^{(\mathrm{cc})}\mathbf{A}_{\mathrm{I}}^{(\mathrm{c})} = \mathbf{U}_{\mathrm{I}}^{(\mathrm{c})}, \tag{24}$$

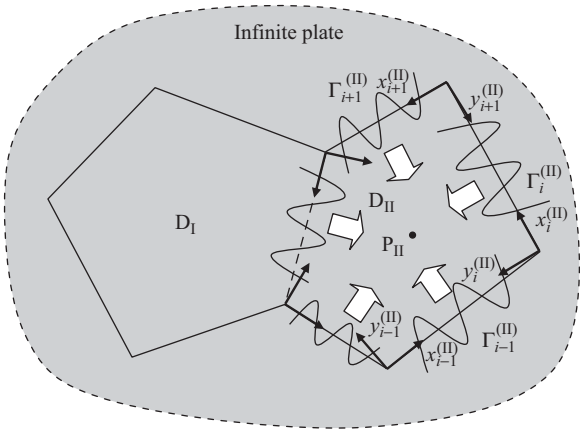


**Fig. 4.** Plane waves simultaneously generated at all edges $\Gamma_1^{(II)}, \Gamma_2^{(II)}, \ldots, \Gamma_{Nb}^{(II)}$ of domain $D_{II}$.

where superscript b represents the real edges ($\Gamma_1^{(I)}, \Gamma_2^{(I)}, \ldots, \Gamma_{Na-1}^{(I)}$) and superscript c represents the common interface ($\Gamma_{Na}^{(I)}$) and

$$\mathbf{SM}_I^{(bb)} = \begin{bmatrix} \mathbf{SM}_I^{(1,1)} & \mathbf{SM}_I^{(1,2)} & \cdots & \mathbf{SM}_I^{(1,Na)} \\ \mathbf{SM}_I^{(2,1)} & \mathbf{SM}_I^{(2,2)} & \cdots & \mathbf{SM}_I^{(2,Na)} \\ \vdots & \vdots & \ddots & \vdots \\ \mathbf{SM}_I^{(Na,1)} & \mathbf{SM}_I^{(Na,2)} & \cdots & \mathbf{SM}_I^{(Na-1,Na-1)} \end{bmatrix}, \tag{25}$$

$$\mathbf{SM}_I^{(bc)} = \begin{bmatrix} \mathbf{SM}_I^{(1,Na)} \\ \mathbf{SM}_I^{(2,Na)} \\ \vdots \\ \mathbf{SM}_I^{(Na-1,Na)} \end{bmatrix}, \tag{26}$$

$$\mathbf{SM}_I^{(cb)} = [\mathbf{SM}_I^{(Na,1)} \ \mathbf{SM}_I^{(Na,2)} \ \cdots \ \mathbf{SM}_I^{(Na,Na-1)}], \tag{27}$$

$$\mathbf{SM}_I^{(cc)} = [\mathbf{SM}_I^{(Na,Na)}], \tag{28}$$

$$\mathbf{A}_I^{(b)} = \{\mathbf{A}_I^{(1)} \ \mathbf{A}_I^{(2)} \ \cdots \ \mathbf{A}_I^{(Na-1)}\}^T, \tag{29}$$

$$\mathbf{A}_I^{(c)} = \{\mathbf{A}_I^{(Na)}\}^T, \tag{30}$$

$$\mathbf{U}_I^{(b)} = \{\mathbf{U}_I^{(1)} \ \mathbf{U}_I^{(2)} \ \cdots \ \mathbf{U}_I^{(Na-1)}\}^T, \tag{31}$$

$$\mathbf{U}_I^{(c)} = \{\mathbf{U}_I^{(Na)}\}^T. \tag{32}$$

*2.2.2. System matrix equation for sub-domain* $D_{II}$

In the section, a system matrix equation for domain $D_{II}$ is extracted in the same manner as for domain $D_I$. (Note that the system matrix equations for domain $D_I$ are given by Eqs. (23) and (24).) First, it is assumed that plane waves are simultaneously generated at all edges of domain $D_{II}$ as shown in Fig. 4. A displacement response at point $P_{II}$ in domain $D_{II}$ is given by superposing displacements that have resulted from the plane waves as follows:

$$W^{(II)} = \sum_{i=1}^{Nb} W_i^{(II)}(x_i^{(II)}, y_i^{(II)}) = \sum_{i=1}^{Nb} \sum_{m=1}^{Ns} B_m^{(i)} \sin\frac{m\pi x_i^{(II)}}{L_i^{(II)}} \exp\left(j\sqrt{\Lambda^2 - \left(\frac{m\pi}{L_i^{(II)}}\right)^2}\, y_i^{(II)}\right), \tag{33}$$

where $B_m^{(i)}$ indicates unknown coefficients associated with the vibration amplitude of the plane wave; $x_i^{(II)}$ and $y_i^{(II)}$ denote local rectangular coordinates defined at edge $\Gamma_i^{(II)}$ as shown in Fig. 4; $L_i^{(II)}$ and $Nb$ represent the length of edge $\Gamma_i^{(II)}$and the

number of edges (including $\Gamma_c$) of domain $D_{II}$, respectively. Furthermore, displacements at edges (including $\Gamma_c$) of domain $D_{II}$ are provisionally assumed as (in the same way as for domain $D_I$)

$$W^{(II)}(x_r^{(II)}, y_r^{(II)} = 0) = \sum_{n=1}^{Ns} V_n^{(r)} \sin\frac{n\pi x_r^{(II)}}{L_r^{(II)}}, \quad r = 1, 2, \ldots, Nb, \tag{34}$$

where $(x_r^{(II)}, y_r^{(II)})$ is the local rectangular coordinates defined at the $r$th edge ($\Gamma_r^{(II)}$), $V_n^{(r)}$ denotes unknown coefficients and $L_r^{(II)}$ is the length of edge $\Gamma_r^{(II)}$.

If substituting Eq. (33) into Eq. (34) and repeating the same procedure (Eqs. (11)–(24)) as performed for domain $D_I$ to domain $D_{II}$, one can obtain two system matrix equations as follows:

$$\mathbf{SM}_{II}^{(bb)}\mathbf{B}_{II}^{(b)} + \mathbf{SM}_{II}^{(bc)}\mathbf{B}_{II}^{(c)} = \mathbf{V}_{II}^{(b)}, \tag{35}$$

$$\mathbf{SM}_{II}^{(cb)}\mathbf{B}_{II}^{(b)} + \mathbf{SM}_{II}^{(cc)}\mathbf{B}_{II}^{(c)} = \mathbf{V}_{II}^{(c)}. \tag{36}$$

### 2.3. Assembling of system matrix equations

In the section, in order to obtain a single system matrix for the concave polygonal plate corresponding to the entire domain ($D_I$+$D_{II}$), the condition of continuity in displacement and slope at the common interface is considered. Concretely speaking, the condition of continuity means that displacement and slope at the common interface for $D_I$ are equal to those for $D_{II}$, respectively.

Prior to considering the condition of continuity, it should be noted in Eqs. (23) and (35) that $\mathbf{U}_I^{(b)} = \mathbf{0}$ and $\mathbf{V}_{II}^{(b)} = \mathbf{0}$ because displacements are equal to zero at fixed edges of two domains $D_I$ and $D_{II}$ excepting the common interface. From this fact, Eqs. (23) and (35) may be changed into, respectively,

$$\mathbf{A}_I^{(b)} = -\mathbf{SM}_I^{(bb)^{-1}}\mathbf{SM}_I^{(bc)}\mathbf{A}_I^{(c)}, \tag{37}$$

$$\mathbf{B}_{II}^{(b)} = -\mathbf{SM}_{II}^{(bb)^{-1}}\mathbf{SM}_{II}^{(bc)}\mathbf{B}_{II}^{(c)}. \tag{38}$$

Substituting Eqs. (37) and (38) into Eqs. (24) and (36) leads to

$$(-\mathbf{SM}_I^{(cb)}\mathbf{SM}_I^{(bb)^{-1}}\mathbf{M}_I^{(bc)} + \mathbf{SM}_I^{(cc)})\mathbf{A}_I^{(c)} = \mathbf{U}_I^{(c)}, \tag{39}$$

$$(-\mathbf{SM}_{II}^{(cb)}\mathbf{SM}_{II}^{(bb)^{-1}}\mathbf{SM}_{II}^{(bc)} + \mathbf{SM}_{II}^{(cc)})\mathbf{B}_{II}^{(c)} = \mathbf{V}_{II}^{(c)}. \tag{40}$$

#### 2.3.1. Condition of continuity in displacement

Thanks to the condition of continuity in displacement at the common interface, it may be said that a displacement at $\Gamma_{Na}^{(I)}$ ($= \Gamma_c$) given by Eq. (10) is equal to a displacement at $\Gamma_{Nb}^{(II)}$ ($= \Gamma_c$) given by Eq. (34), i.e.,

$$\sum_{n=1}^{Ns} U_n^{(Na)} \sin\frac{n\pi x_{Na}^{(I)}}{L_{Na}^{(I)}} = \sum_{n=1}^{Ns} V_n^{(Nb)} \sin\frac{n\pi x_{Nb}^{(II)}}{L_{Nb}^{(I)}}. \tag{41}$$

From Eq. (41), the condition of continuity in displacement is reduced to

$$U_n^{(Na)} = (-1)^{n+1} V_n^{(Nb)}, \quad n = 1, 2, \ldots, Ns, \tag{42}$$

where $(-1)^{n+1}$ results from the fact that the origin and direction of $x_{Na}^{(I)}$ are different from those of $x_{Nb}^{(II)}$ at common interface $\Gamma_c$. Eq. (42) may be rewritten as matrix form

$$\mathbf{U}_I^{(c)} = (-1)^{n+1}\mathbf{V}_{II}^{(c)}. \tag{43}$$

If Eq. (43) is applied to Eqs. (39) and (40), one can obtain

$$(-\mathbf{SM}_I^{(cb)}\mathbf{SM}_I^{(bb)^{-1}}\mathbf{SM}_I^{(bc)} + \mathbf{SM}_I^{(cc)})\mathbf{A}_I^{(c)} + (-1)^{n+1}(\mathbf{SM}_{II}^{(cb)}\mathbf{SM}_{II}^{(bb)^{-1}}\mathbf{SM}_{II}^{(bc)} - \mathbf{SM}_{II}^{(cc)})\mathbf{B}_{II}^{(c)} = \mathbf{0}. \tag{44}$$

#### 2.3.2. Condition of continuity in slope

First, slopes of the two domains $D_I$ and $D_{II}$ at the common interface are, respectively, assumed as a linear combination of sine series (in the same manner as in Eqs. (10) and (34)), i.e.,

$$\frac{\partial W^{(I)}}{\partial y_{Na}^{(I)}}(x_{Na}^{(I)}, y_{Na}^{(I)} = 0) = \sum_{n=1}^{Ns} \bar{U}_n^{(Na)} \sin\frac{n\pi x_{Na}^{(I)}}{L_{Na}^{(I)}} \quad \text{for } D_I, \tag{45}$$

$$\frac{\partial W^{(\mathrm{II})}}{\partial y_{Nb}^{(\mathrm{II})}}(x_{Nb}^{(\mathrm{II})}, y_{Nb}^{(\mathrm{II})}=0)=\sum_{n=1}^{Ns}\bar{V}_n^{(Nb)}\sin\frac{n\pi x_{Nb}^{(\mathrm{II})}}{L_{Nb}^{(\mathrm{II})}} \quad \text{for } \mathrm{D_{II}}, \tag{46}$$

where $\bar{U}_n^{(Na)}$ and $\bar{V}_n^{(Nb)}$ denote unknown coefficients. Similarly, if substituting the approximate solution equations (7) and (33) into Eqs. (45) and (46), respectively, and repeating the same procedure as Eqs. (11)–(22), (45) and (46) lead to, respectively,

$$\sum_{i=1}^{Na-1}\left(\sum_{m=1}^{Ns}A_m^{(i)}\overline{SM}_{\mathrm{I}_{(q,m)}}^{(i,Na)}\right)+\sum_{m=1}^{Ns}A_m^{(Na)}\overline{SM}_{\mathrm{I}_{(q,m)}}^{(Na,Na)}=\bar{U}_q^{(Na)}, \quad q=1,2,\ldots,Ns, \tag{47}$$

$$\sum_{i=1}^{Nb-1}\left(\sum_{m=1}^{Ns}B_m^{(i)}\overline{SM}_{\mathrm{II}_{(q,m)}}^{(i,Nb)}\right)+\sum_{m=1}^{Ns}B_m^{(Nb)}\overline{SM}_{\mathrm{II}_{(q,m)}}^{(Nb,Nb)}=\bar{V}_q^{(Nb)}, \quad q=1,2,\ldots,Ns, \tag{48}$$

where $\overline{SM}_{\mathrm{I}_{(q,m)}}^{(i,Na)}$ is given by

$$SM_{\mathrm{I}_{(q,m)}}^{(i,Na)}=\frac{2}{L_r^{(\mathrm{I})}}\int_0^{L_r^{(\mathrm{I})}}\frac{\partial}{\partial x_r^{(\mathrm{I})}}\left[\sin\frac{m\pi f_{ir}^{(\mathrm{I})}(x_r^{(\mathrm{I})},y_r^{(\mathrm{I})}=0)}{L_i^{(\mathrm{I})}}\exp\left(\mathrm{j}\sqrt{\Lambda^2-\left(\frac{m\pi}{L_i^{(\mathrm{I})}}\right)^2}\,g_{ir}^{(\mathrm{I})}(x_r^{(\mathrm{I})},y_r^{(\mathrm{I})}=0)\right)\sin\frac{q\pi x_r^{(\mathrm{I})}}{L_r^{(\mathrm{I})}}\right]\mathrm{d}x_r^{(\mathrm{I})} \tag{49}$$

and $\overline{SM}_{\mathrm{II}_{(q,m)}}^{(i,Nb)}$ may be obtained by replacing subscript I and superscript *Na* in Eq. (49) by II and *Nb*, respectively.

Furthermore, Eqs. (47) and (48) may be simply, respectively, expressed in the form of system matrix equations as follows:

$$\overline{\mathbf{SM}}_{\mathrm{I}}^{(\mathrm{cb})}\mathbf{A}_{\mathrm{I}}^{(\mathrm{b})}+\overline{\mathbf{SM}}_{\mathrm{I}}^{(\mathrm{cc})}\mathbf{A}_{\mathrm{I}}^{(\mathrm{c})}=\bar{\mathbf{U}}_{\mathrm{I}}^{(\mathrm{c})}, \tag{50}$$

$$\overline{\mathbf{SM}}_{\mathrm{II}}^{(\mathrm{cb})}\mathbf{B}_{\mathrm{II}}^{(\mathrm{b})}+\overline{\mathbf{SM}}_{\mathrm{II}}^{(\mathrm{cc})}\mathbf{B}_{\mathrm{II}}^{(\mathrm{c})}=\bar{\mathbf{V}}_{\mathrm{II}}^{(\mathrm{c})}, \tag{51}$$

where $\bar{\mathbf{U}}_{\mathrm{I}}^{(\mathrm{c})}=(-1)^n\bar{\mathbf{V}}_{\mathrm{II}}^{(\mathrm{c})}$ due to the condition of continuity in slope in the common interface. Note that $(-1)^n$ results from the fact that the direction of $y_{Na}^{(\mathrm{I})}$ is opposite to that of $y_{Nb}^{(\mathrm{II})}$ as well as the origin and direction of $x_{Na}^{(\mathrm{I})}$ are different from those of $x_{Nb}^{(\mathrm{II})}$ at common interface $\Gamma_c$.

Next, if substituting Eqs. (37) and (38) into Eqs. (50) and (51) and considering $\bar{\mathbf{U}}_{\mathrm{I}}^{(\mathrm{c})}=(-1)^n\bar{\mathbf{V}}_{\mathrm{II}}^{(\mathrm{c})}$, Eqs. (50) and (51) are reduced to

$$(-\overline{\mathbf{SM}}_{\mathrm{I}}^{(\mathrm{cb})}\mathbf{SM}_{\mathrm{I}}^{(\mathrm{bb})^{-1}}\mathbf{SM}_{\mathrm{I}}^{(\mathrm{bc})}+\overline{\mathbf{SM}}_{\mathrm{I}}^{(\mathrm{cc})})\mathbf{A}_{\mathrm{I}}^{(\mathrm{c})}+(-1)^n(\overline{\mathbf{SM}}_{\mathrm{II}}^{(\mathrm{cb})}\mathbf{SM}_{\mathrm{II}}^{(\mathrm{bb})^{-1}}\mathbf{SM}_{\mathrm{II}}^{(\mathrm{bc})}-\overline{\mathbf{SM}}_{\mathrm{II}}^{(\mathrm{cc})})\mathbf{B}_{\mathrm{II}}^{(\mathrm{c})}=\mathbf{0}. \tag{52}$$

### 2.3.3. System matrix equation of the entire domain

Finally, Eqs. (44) and (52) may take the form of a single matrix equation:

$$\mathbf{SM}(f)\mathbf{C}=\mathbf{0}, \tag{53}$$

where the system matrix $\mathbf{SM}(f)$, which is a function of the frequency $f$, and the unknown coefficient vector $\mathbf{C}$ are given by

$$\mathbf{SM}=\begin{bmatrix}-\mathbf{SM}_{\mathrm{I}}^{(\mathrm{cb})}\mathbf{SM}_{\mathrm{I}}^{(\mathrm{bb})^{-1}}\mathbf{SM}_{\mathrm{I}}^{(\mathrm{bc})}+\mathbf{SM}_{\mathrm{I}}^{(\mathrm{cc})} & (-1)^n(\mathbf{SM}_{\mathrm{II}}^{(\mathrm{cb})}\mathbf{SM}_{\mathrm{II}}^{(\mathrm{bb})^{-1}}\mathbf{SM}_{\mathrm{II}}^{(\mathrm{bc})}-\mathbf{SM}_{\mathrm{II}}^{(\mathrm{cc})})\\ -\overline{\mathbf{SM}}_{\mathrm{I}}^{(\mathrm{cb})}\mathbf{SM}_{\mathrm{I}}^{(\mathrm{bb})^{-1}}\mathbf{SM}_{\mathrm{I}}^{(\mathrm{bc})}+\overline{\mathbf{SM}}_{\mathrm{I}}^{(\mathrm{cc})} & (-1)^n(\overline{\mathbf{SM}}_{\mathrm{II}}^{(\mathrm{cb})}\mathbf{SM}_{\mathrm{II}}^{(\mathrm{bb})^{-1}}\mathbf{SM}_{\mathrm{II}}^{(\mathrm{bc})}-\overline{\mathbf{SM}}_{\mathrm{II}}^{(\mathrm{cc})})\end{bmatrix}, \tag{54}$$

$$\mathbf{C}=\begin{Bmatrix}\mathbf{A}_{\mathrm{I}}^{(\mathrm{c})}\\ \mathbf{B}_{\mathrm{II}}^{(\mathrm{c})}\end{Bmatrix}. \tag{55}$$

On the other hand, the natural frequencies of the concave polygonal plate may be found from the non-trivial condition that the solution of Eq. (53) should not be zero (i.e., $\mathbf{C}\neq\mathbf{0}$). As the result, the natural frequencies are given by the roots of the determinant equation $\mathrm{def}[\mathbf{SM}(f)]=0$.

In addition, the $i$th mode shape for the $i$th natural frequencies, $f_i$, may be plotted from Eqs. (7) and (33). For this, $\mathbf{A}_{\mathrm{I}}^{(\mathrm{c})}$ and $\mathbf{B}_{\mathrm{II}}^{(\mathrm{c})}$ of the unknown coefficients included in the equations can be obtained from the $i$th eigenvector obtained from Eq. (53) when $f=f_i$. In addition, $\mathbf{A}_{\mathrm{I}}^{(\mathrm{b})}$ and $\mathbf{B}_{\mathrm{II}}^{(\mathrm{b})}$ of the unknown coefficients included in Eqs. (7) and (33) can be calculated by substituting $\mathbf{A}_{\mathrm{I}}^{(\mathrm{c})}$ and $\mathbf{B}_{\mathrm{II}}^{(\mathrm{c})}$ into Eqs. (37) and (38), respectively.

## 3. Case studies

In this section, several case studies are presented to verify the validity of the proposed method. For each case, the natural frequencies and mode shapes obtained are compared with those given by another analytical method (NDIF method) or FEM (NASTRAN). The case studies show that the present method is very accurate and effective, especially when it is used for a concavely shaped plate with high concavity. Note that the physical properties of plates used in the case studies are as follows: $E = 2.068 \times 10^{11}\,\mathrm{N/m^2}$, $\nu = 0.29$, $h = 0.005\,\mathrm{m}$ and $\rho = \rho_s/h = 7820\,\mathrm{kg/m^3}$.

### 3.1. Rectangular plate

In order to verify the accuracy of the proposed method, a rectangular plate with exact natural frequencies is solved by the method. As shown in Fig. 5, the rectangular plate is intentionally divided into two regions whose interface is oblique.

Natural frequencies of the rectangular plate are given by the values of the frequency $f$ corresponding to the troughs that appear in the logarithm determinant curve in Fig. 6 where the curve is given by plotting $\log|\det[\mathbf{SM}(f)]|$ as a function of $f$. Natural frequencies for $N_s = 4$, 6 and 8 by the proposed method are summarized in Table 1 where the exact natural frequencies and the natural frequencies obtained by FEM (NASTRAN) are also presented. It may be said from Table 1 that the proposed method gives very accurate natural frequencies although a small number of basis functions are used, and that the natural frequencies by the proposed method rapidly converge to the exact solutions. (Note that natural frequencies by FEM using 1089 nodes do not converge to the exact natural frequencies.) On the other hand, although not plotted here, the mode shapes obtained from the present method and FEM (NASTRAN) are confirmed to be in good agreement.

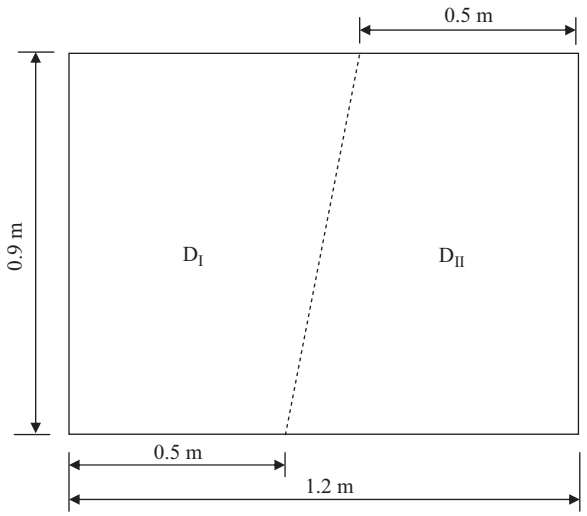


**Fig. 5.** Rectangular plate divided into two domains whose interface is oblique.

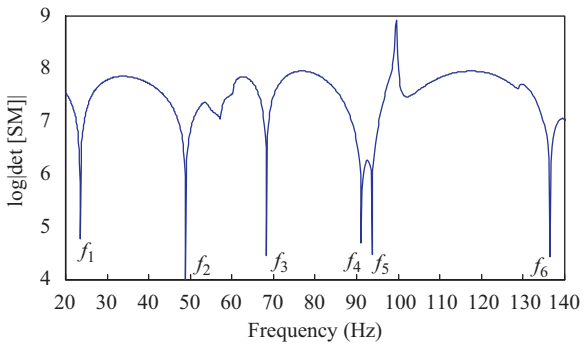


**Fig. 6.** Logarithm determinant curve of the rectangular plate for $N_s = 6$.

**Table 1**
Comparison of natural frequencies (Hz) of the rectangular plate obtained by the present method, the exact method [34] and FEM.

| Natural frequencies | Proposed method | | | Exact solution [34] | FEM (NASTRAN) | | |
|---|---|---|---|---|---|---|---|
| | $N_s = 4$ | $N_s = 6$ | $N_s = 8$ | | 1089 nodes | 289 nodes | 49 nodes |
| $f_1$ | 23.58 | 23.50 | 23.50 | 23.50 | 23.52 | 23.58 | 24.05 |
| $f_2$ | 48.84 | 48.89 | 48.89 | 48.89 | 49.01 | 49.37 | 52.43 |
| $f_3$ | 68.15 | 68.34 | 68.63 | 68.63 | 68.83 | 69.44 | 74.50 |
| $f_4$ | 91.10 | 91.10 | 91.20 | 91.20 | 91.76 | 93.47 | 102.9 |
| $f_5$ | 93.44 | 93.66 | 94.02 | 94.02 | 94.32 | 95.23 | 108.0 |
| $f_6$ | 136.4 | 136.4 | 136.3 | 136.3 | 137.1 | 139.3 | 158.4 |

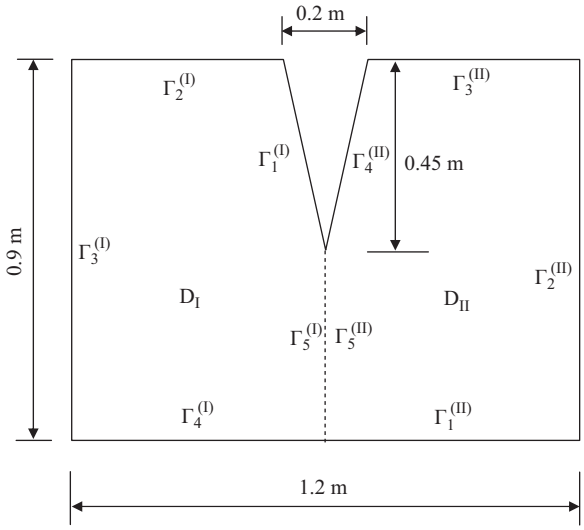


**Fig. 7.** Highly concave plate divided into two domains.

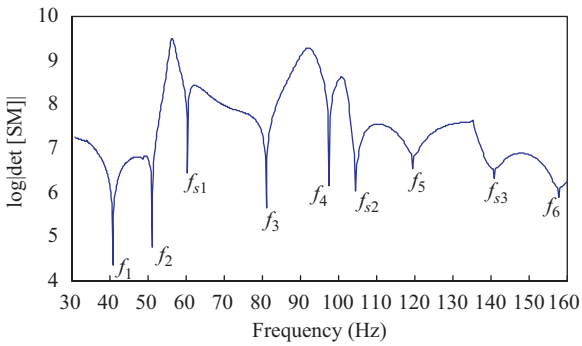


**Fig. 8.** Logarithm determinant curve of the highly concave plate for $N_s = 6$ (spurious natural frequencies: $f_{s1} = 60.16$, $f_{s2} = 104.5$, $f_{s3} = 140.8$ Hz).

### 3.2. Highly concave plate

In order to show the validity of the proposed method for a concavely shaped plate with high concavity, it is applied to a rectangular plate with a partially concave region shown in Fig. 7. The determinant curve of $\log|\det[\mathbf{SM}(f)]|$ for $N_s = 6$ is shown in Fig. 8 where the troughs ($f_1 f_2, \ldots f_6$) represent the first six natural frequencies of the plate. Natural frequencies for $N_s = 4$, 6, 8, 10 and 12 are tabulated in Table 2 from which it may be said that these natural frequencies agree well with those calculated by NDIF method [3] and FEM (NASTRAN). Also, it is confirmed that the proposed method shows an excellent convergence feature when $N_s$ is increased from $N_s = 4$ to 12. Although analysis results for more than $N_s = 12$ are

**Table 2**
Comparison of natural frequencies (Hz) of the highly concave rectangular plate obtained by the present method, the NDIF method and FEM.

| Natural frequencies | Proposed method | | | | | NDIF method [3] (30 nodes) | FEM (NASTRAN) | | |
|---|---|---|---|---|---|---|---|---|---|
| | $N_s=4$ | $N_s=6$ | $N_s=8$ | $N_s=10$ | $N_s=12$ | | 1701 nodes | 976 nodes | 451 nodes |
| $f_1$ | 41.24 | 40.82 | 40.68 | 40.53 | 40.53 | 41.39 | 40.25 | 40.39 | 40.68 |
| $f_2$ | 51.20 | 51.04 | 51.04 | 51.04 | 51.04 | 50.88 | 50.88 | 51.04 | 51.20 |
| $f_3$ | 80.80 | 81.00 | 81.20 | 81.24 | 81.39 | 82.00 | 82.41 | 82.61 | 83.21 |
| $f_4$ | 97.57 | 97.57 | 97.57 | 97.56 | 97.56 | 97.35 | 97.57 | 97.79 | 98.23 |
| $f_5$ | 119.8 | 119.5 | 119.5 | 119.5 | 119.5 | 121.5 | 120.3 | 120.8 | 122.0 |
| $f_6$ | 158.2 | 157.6 | 157.4 | 157.0 | 157.0 | 156.3 | 157.9 | 158.8 | 161.3 |

not presented, the results also show good convergence characteristics. In addition, although mode shapes by the present method are omitted in the paper, they are in good agreement with mode shapes by FEM.

On the other hand, it should be noticed that spurious natural frequencies ($f_{s1}$, $f_{s2}$ and $f_{s3}$) as well as the real natural frequencies ($f_1, f_2, \ldots f_6$) of the plate appear in the determinant curve shown in Fig. 8. The spurious natural frequencies may result from the functional dependence between plane waves used as basis functions. For example, the 1st spurious natural frequency $f_{s1}=60.15$ Hz, which is calculated as $\Lambda_{s1}=6.98$ by Eq. (5), corresponds to the cut-off frequency of the 2nd plane wave generated at edge $\Gamma_3^{(\mathrm{I})}$ or that of the 1st plane wave generated at edge $\Gamma_5^{(\mathrm{I})}$. From Eq. (6), the two plane waves may be expressed as, respectively,

$$A_2^{(3)}\sin\frac{2\pi x_3^{(\mathrm{I})}}{L_3^{(\mathrm{I})}}\exp\left(j\sqrt{\Lambda^2-\left(\frac{2\pi}{L_3^{(\mathrm{I})}}\right)^2}\,y_3^{(\mathrm{I})}\right), \tag{56}$$

$$A_1^{(5)}\sin\frac{\pi x_5^{(\mathrm{I})}}{L_5^{(\mathrm{I})}}\exp\left(\mathrm{j}\sqrt{\Lambda^2-\left(\frac{\pi}{L_5^{(\mathrm{I})}}\right)^2}\,y_5^{(\mathrm{I})}\right). \tag{57}$$

As a result, at cut-off frequency $f_{s1}$, the two plane waves are reduced to, respectively,

$$A_2^{(3)}\sin\frac{2\pi x_3^{(\mathrm{I})}}{L_3^{(\mathrm{I})}}, \tag{58}$$

$$A_1^{(5)}\sin\frac{\pi x_5^{(\mathrm{I})}}{L_5^{(\mathrm{I})}}. \tag{59}$$

If considering $x_3^{(\mathrm{I})}=L_3^{(\mathrm{I})}-x_5^{(\mathrm{I})}$ and $L_3^{(\mathrm{I})}=2L_5^{(\mathrm{I})}$, Eqs. (58) and (59) lead to, respectively,

$$-A_2^{(3)}\sin\frac{\pi x_5^{(\mathrm{I})}}{L_5^{(\mathrm{I})}}, \tag{60}$$

$$A_1^{(5)}\sin\frac{\pi x_5^{(\mathrm{I})}}{L_5^{(\mathrm{I})}}. \tag{61}$$

Finally, it may be confirmed from Eqs. (60) and (61) that the two plane waves are functionally dependent (are equal). Due to this functional dependence, the system matrix **SM** becomes singular at the cut-off frequency and, as the result, the spurious natural frequency is created in the determinant curve shown in Fig. 8.

In the paper, mode shapes are plotted to discern real natural frequencies from spurious ones because meaningless mode shapes are plotted for spurious natural frequencies. On the other hand, the authors are carrying out an additional study for effectively removing the spurious natural frequencies in the determinant curve.

### 3.3. General quadrilateral plate

As shown in Fig. 9, a general quadrilateral plate is divided into two regions and is solved for $N_s=4$, 6 and 8. The logarithm determinant curves for $N_s=6$ is shown in Fig. 10 where it may be found that six real natural frequencies and three spurious ones are marked. As indicated in the previous case study, the spurious natural frequencies result from the functional dependence between basis functions used and are distinguished from real natural frequencies by plotting mode shapes. The first six natural frequencies obtained by the proposed method are summarized in Table 3 where it may be seen

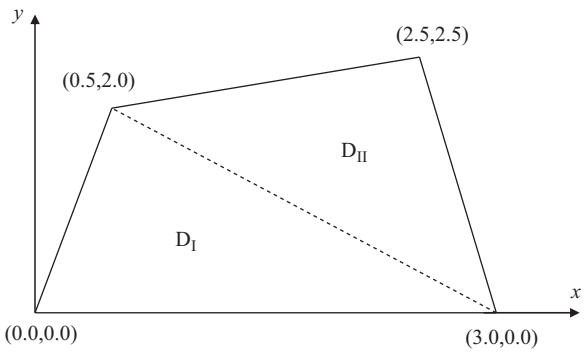


**Fig. 9.** General quadrilateral plate divided into two domains.

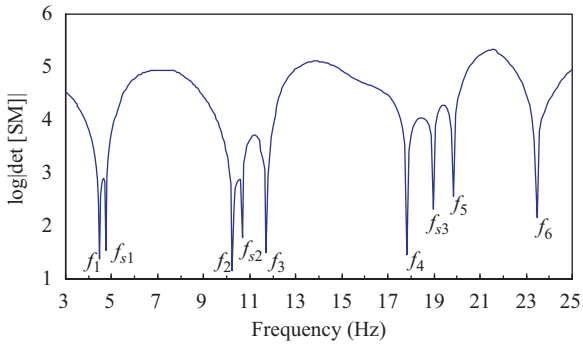


**Fig. 10.** Logarithm determinant curve of the general quadrilateral plate for $N_s = 6$ (spurious natural frequencies: $f_{s1} = 4.743$, $f_{s2} = 10.67$, $f_{s3} = 18.97$ Hz).

**Table 3**
Comparison of natural frequencies (Hz) of the general quadrilateral plate obtained by the present method and FEM.

| Natural frequencies | Proposed method | | | FEM (NASTRAN) | | |
|---|---|---|---|---|---|---|
| | $N_s = 4$ | $N_s = 6$ | $N_s = 8$ | 1812 nodes | 1060 nodes | 438 nodes |
| $f_1$ | 4.457 | 4.557 | 4.457 | 4.410 | 4.410 | 4.410 |
| $f_2$ | 10.24 | 10.24 | 10.24 | 10.24 | 10.24 | 10.17 |
| $f_3$ | 11.71 | 11.71 | 11.71 | 11.71 | 11.71 | 11.64 |
| $f_4$ | 17.83 | 17.83 | 17.83 | 17.83 | 17.73 | 17.55 |
| $f_5$ | 19.65 | 19.65 | 19.65 | 19.75 | 19.65 | 19.65 |
| $f_6$ | 23.36 | 23.47 | 23.47 | 23.36 | 23.36 | 23.25 |

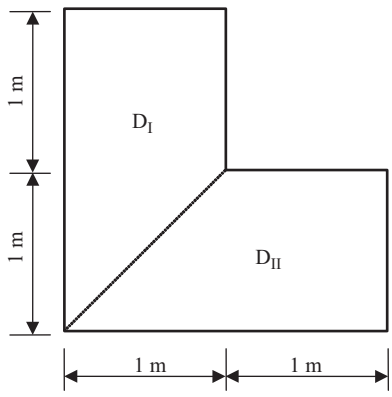


**Fig. 11.** L-shaped plate divided into two domains.

**Table 4**
Comparison of natural frequencies (Hz) of the L-shaped plate obtained by the present method, FEM and Milsted's method [35].

| Natural frequencies | Proposed method | | | FEM (NASTRAN) (1302 nodes) | Milsted's method [35] |
|---|---|---|---|---|---|
| | $N_s = 8$ | $N_s = 10$ | $N_s = 12$ | | |
| $f_1$ | 11.79 | 11.86 | 11.86 | 11.94 | 11.94 |
| $f_2$ | 19.07 | 19.07 | 19.07 | 18.78 | 18.78 |
| $f_3$ | 24.56 | 24.56 | 24.56 | 24.45 | 24.34 |
| $f_4$ | 36.67 | 36.67 | 36.67 | 36.54 | 36.54 |
| $f_5$ | 38.85 | 38.99 | 38.99 | 39.69 | 41.96 |
| $f_6$ | 51.68 | 51.68 | 51.68 | 51.68 | N/P |

N/P denotes 'not presented'.

that the method has an excellent convergence feature as the number of $N_s$ increases and it yields very accurate results close to those computed by FEM.

### 3.4. L-shaped plate

A L-shaped plate, which is frequently used as an example of concave plates in other papers, is considered in the section. The plate is divided into two regions as shown in Fig. 11 and is solved for $N_s = 8$, 10 and 12. Table 4 shows that the natural frequencies by the proposed method agree well with those by FEM as well as Milsted's method [35], which uses a semi-analytical approach. In Table 4, it may be seen that the proposed has a good convergence feature.

## 4. Conclusions

An effective, analytical sub-domain method for the free vibration analysis of simply supported polygonal plates with arbitrary shapes was proposed in the paper. It was revealed that the method shows an excellent convergence feature and gives accurate natural frequencies and mode shapes for not only general polygonal plates but also highly concave polygonal plates that rarely have been dealt with by previous researchers. It is expected that the application region of the method comes up to the free vibration analyses of general polygonal plates with various combinations of the elementary boundary conditions (simply supported, clamped and free boundary conditions).

On the other hand, the proposed method cannot be directly applied to multiply connected plates and polygonal plates with holes because it divides the region of the plate of interest into only two regions. In order to overcome this weak point, an extended way of dividing the region of the plate into many regions will be developed in future research.

## Acknowledgement

This work was supported by the Korea Research Foundation Grant funded by the Korean Government (MOEHRD, Basic Research Promotion Fund) (KRF-2007-013-D00006).

## References

[1] S.W. Kang, J.M. Lee, Y.J. Kang, Vibration analysis of arbitrarily shaped membranes using non-dimensional dynamic influence function, *Journal of Sound and Vibration* 221 (1999) 117–132.
[2] S.W. Kang, J.M. Lee, Eigenmode analysis of arbitrarily shaped two-dimensional cavities by the method of point-matching, *Journal of the Acoustical Society of America* 107 (3) (2000) 1153–1160.
[3] S.W. Kang, J.M. Lee, Application of free vibration analysis of membranes using the non-dimensional dynamic influence function, *Journal of Sound and Vibration* 234 (3) (2000) 455–470.
[4] S.W. Kang, J.M. Lee, Free vibration analysis of arbitrarily shaped plates with clamped edges using wave-type functions, *Journal of Sound and Vibration* 242 (1) (2002) 9–26.
[5] S.W. Kang, Free vibration analysis of arbitrarily shaped plates with a mixed boundary condition using non-dimensional dynamic influence functions, *Journal of Sound and Vibration* 256 (3) (2002) 533–549.
[6] S.W. Kang, S.H. Kim, Free vibration analysis of free plates with smoothly varying boundary shapes using non-dimensional dynamic influence functions, *Journal of Vibration and Acoustics—Transactions of the ASME* 130 (4) (2008) 1–8 (041010).
[7] B. Singh, S. Chakraverty, Transverse vibration of simply supported elliptical and circular plates using boundary characteristic orthogonal polynomials in two variables, *Journal of Sound and Vibration* 152 (1) (1992) 149–155.
[8] H.D. Conway, K.A. Karnham, The free flexural vibration of triangular rhombic and parallelogram plates and some anologies, *International Journal of Mechanical Sciences* 7 (1965) 811–816.
[9] S. Durvasula, Free vibration of simply supported parallelogrammic plates, *Journal of Aircraft* 6 (1969) 66–68.
[10] I. Chopra, S. Durvasula, Vibration of simply supported trapezoidal plates, I. Symmetric trapezoids, *Journal of Sound and Vibration* 19 (1972) 379–392.
[11] I. Chopra, S. Durvasula, Vibration of simply supported trapezoidal plates, II. Unsymmetric trapezoids, *Journal of Sound and Vibration* 20 (1972) 125–134.
[12] S. Durvasula, Natural frequencies and modes of skew membranes, *Journal of the Acoustical Society of America* 44 (1968) 1636–1646.
[13] S. Durvasula, Natural frequencies and modes of clamped skew plates, *American Institute of Aeronautics and Astronautics Journal* 7 (1969) 1164–1167.

[14] M. Hasegwa, Vibration of clamped parallelogrammic isotropic flat plates, *Journal of the Aeronautical Sciences* 24 (1957) 145–146.
[15] M. Hamada, Compressive or shear buckling load and fundamental frequency of a rhomboidal plate with all edges clamped, *Bulletin of the Japan Society of Mechanical Engineers* 2 (1959) 520–526.
[16] P.S. Nair, S. Durvasula, Vibration of skew plates, *Journal of Sound and Vibration* 26 (1973) 1–19.
[17] S.M. Dickinson, The buckling and frequency of flexural vibration of rectangular isotropic and orthotropic plates using Rayleigh's method, *Journal of Sound and Vibration* 61 (1978) 1–8.
[18] A.W. Lessia, The free vibration of rectangular plates, *Journal of Sound and Vibration* 31 (1973) 257–293.
[19] K. Sato, Free-flexural vibrations of an elliptical plate with free edges, *Journal of the Acoustical Society of America* 54 (1973) 547–550.
[20] L. Meirovitch, *Analytical Methods in Vibrations*, Macmillan Publishing, New York, 1967, pp. 179–189.
[21] D. Blevins, *Formulas for Natural Frequency and Mode Shape*, Van Nostrand-Reinhold, New York, 1979, pp. 233–239.
[22] T. Irie, G. Yamada, K. Umesato, Free vibration of regular polygonal plates with simply supported edges, *Journal of the Acoustical Society of America* 69 (5) (1981) 1330–1336.
[23] H.D. Conway, The bending, buckling, and flexural vibration of simply supported polygonal plates by point-matching, *American Society of Mechanical Engineers—Journal of Applied Mechanics* 28 (1961) 288–291.
[24] J. Mazumdar, Transverse vibration of membranes of arbitrary shape by the method of constant-deflection contours, *Journal of Sound and Vibration* 27 (1973) 47–57.
[25] K. Nagaya, Vibrations and dynamic response of membranes with arbitrary shape, *American Society of Mechanical Engineers—Journal of Applied Mechanics* 45 (1978) 153–158.
[26] Z. Ding, Vibration of arbitrarily shaped membrane carrying elastically mounted masses, *Computers & Structures* 42 (1992) 389–394.
[27] D. Bucco, J. Mazumdar, Vibration analysis of plates of arbitrary shape—a new approach, *Journal of Sound and Vibration* 67 (2) (1979) 253–262.
[28] T.J.R. Hughes, *The Finite Element Method*, Prentice-Hall, New Jersey, 1987.
[29] C.A. Brebbia, *The Boundary Element Method for Engineers*, Wiley, New York, 1978.
[30] C.A. Brebbia, J.C.F. Telles, L.C. Wrobel, *Boundary Element Techniques*, Springer, New York, 1984.
[31] S.W. Kang, J.M. Lee, Free vibration analysis of composite rectangular membranes with an oblique interface, *Journal of Sound and Vibration* 251 (3) (2002) 505–517.
[32] S.W. Kang, Free vibration analysis of composite rectangular membranes with a bent interface, *Journal of Sound and Vibration* 272 (1) (2004) 39–53.
[33] S.W. Kang, J.M. Lee, Free vibration analysis of an unsymmetric trapezoidal membrane, *Journal of Sound and Vibration* 272 (2) (2004) 450–460.
[34] D.J. Gorman, *Free Vibration Analysis of Rectangular Plates*, North Holland, Inc., New York, 1982, pp. 10–13.
[35] M.G. Milsted, J.R. Hutchinson, Use of trigonometric terms in the finite element with application to vibrating membranes, *Journal of Sound and Vibration* 32 (1974) 327–346.